A Model of Chlorophyll Fluorescence in Microalgae Integrating Photoproduction, Photoinhibition and Photoregulation

Andreas Nikolaou[1,†], Andrea Bernardi[2,†], Andrea Meneghesso[3], Fabrizio Bezzo[2], Tomas Morosinotto[3], Benoit Chachuat[1,*]

[1] Centre for Process Systems Engineering, Department of Chemical Engineering, Imperial College London, UK

[2] CAPE-Lab: Computer-Aided Process Engineering Laboratory and PAR-Lab: Padova Algae Research Laboratory, Department of Industrial Engineering, University of Padova, Italy

[3] PAR-Lab: Padova Algae Research Laboratory, Department of Biology, University of Padova, Italy

[*] Corresponding author · E-mail: b.chachuat@imperial.ac.uk · Tel: +44 207 594 5594 · Address: Department of Chemical Engineering, Imperial College London, South Kensington Campus, London, SW7 2AZ, UK

[†] Equal contributors

Short Title: **Model of Chlorophyll Fluorescence in Microalgae**

Abstract

This paper presents a mathematical model capable of quantitative prediction of the state of the photosynthetic apparatus of microalgae in terms of their open, closed and damaged reaction centers under variable light conditions. This model combines the processes of photoproduction and photoinhibition in the Han model with a novel mathematical representation of photoprotective mechanisms, including qE-quenching and qI-quenching. For calibration and validation purposes, the model can be used to simulate fluorescence fluxes, such as those measured in PAM fluorometry, as well as classical fluorescence indexes. A calibration is carried out for the microalga *Nannochloropsis gaditana*, whereby 9 out of the 13 model parameters are estimated with good statistical significance using the realized, minimal and maximal fluorescence fluxes measured from a typical PAM protocol. The model is further validated by considering a more challenging PAM protocol alternating periods of intense light and dark, showing a good ability to provide quantitative predictions of the fluorescence fluxes even though it was calibrated for a different and somewhat simpler PAM protocol. A promising application of the model is for the prediction of PI-response curves based on PAM fluorometry, together with the long-term prospect of combining it with hydrodynamic and light attenuation models for high-fidelity simulation and optimization of full-scale microalgae production systems.

Keywords

microalgae · dynamic model · PAM fluorometry · photoinhibition · photoregulation · non-photochemical quenching · *Nannochloropsis gaditana*

1. Introduction

The potential of microalgae for biofuel production has long been recognized (Sheehan et al., 1998). Their high productivity, their ability to accumulate triacylglycerols (TAGs) under certain stress conditions, and their independence from arable land and fresh water all together, put them in a competitive position against conventional oil crops (Chisti, 2007; Williams and Laurens, 2010; Mutanda et al., 2011). Nonetheless, the most optimistic previsions are based on crude extrapolations of the productivities obtained in the lab, where conditions differ drastically from those in outdoor culture systems, and no pilot- or larger-scale demonstration plant has been able to reproduce them as of yet. A better understanding of the underlying biophysical processes and their interactions is clearly necessary in order to assess the true potential of microalgae culture systems.

In this context, mathematical modeling can be a great help for developing a better understanding, and in turn enabling a better prediction capability, of microalgae culture dynamics. Models that convey state-of-the-art scientific knowledge are invaluable tools for unveiling and untangling the underlying photosynthetic and metabolic mechanisms. These models can be tested in a systematic way through dedicated experiments and, conversely, they can be used to guide the design of dedicated, information-rich experiments. For process development purposes too, models can be used to improve the design, operation and control of a microalgae culture system in order to enable and sustain a higher productivity or TAG content (Cornet et al., 1992).

Microalgae exhibit a remarkable biological complexity due to the interaction of light- and nutrient-limitation effects that span multiple time scales, ranging from milliseconds to days: *Photoproduction*, namely the collection of all processes from photons utilization to CO_2 fixation, occurs in a fraction of a second (Williams and Laurens, 2010); *Photoinhibition*, the observed loss of photosynthetic production due to excess or prolonged exposure to light, acts on time scales of minutes to hours (Long et al., 1994); *Photoregulation*, also known as *Non Photochemical Quenching* (NPQ), the set of mechanisms by which microalgae protect their photosynthetically-active components via the dissipation of excess energy as heat, also occurs within minutes (Müller et al., 2001); *Photoacclimation*, the ability of microalgae to adjust their pigment content and composition under varying light and nutrient conditions, acts on time scales of hours to days (MacIntyre et al., 2002); and finally, the mechanisms involved in nutrient

internalization and their metabolism into useful products occur within hours to days as well (Falkowski and Raven, 1997).

Among the available experimental tools to study the aforementioned processes, the use of chlorophyll-a fluorescence has led to important discoveries over the past 40 years (Baker, 2008). Today's state-of-the-art equipment, such as *Pulse Amplitude Modulation* (PAM) fluorometers, are not only easy to use and fast, but they can also implement complex protocols with great measurement precision (Huot and Babin, 2010). Traditionally, a number of fluorescence indexes, such as the realized quantum yield of photosynthesis or the NPQ index, have been used for monitoring specific photosynthetic mechanisms, by qualitatively relating these mechanisms to the measured fluorescence fluxes (Roháček, 2002). In contrast, little effort has been devoted to quantifying these relations in the form of mathematical models, which would enable accurate predictions of the quantum yield of photosynthesis and in particular of its dynamic response to variable light conditions. ~~Other prospects for such models include the possibility of predicting photosynthesis-irradiance (PI) curves based solely on fluorescence measurements, and eventually the development of fully-automated, fluorescence-based protocols for detailed screening of the photosynthetic properties of microalgae.~~

The main contributions of this paper are the development of a mathematical model describing the key photosynthetic mechanisms triggered by variable light conditions and its validation using PAM fluorescence experiments. Our model uses the well-accepted model of photoproduction and photoinhibition due to Han (2002) as a building block and it encompasses two types of photoregulation, namely qE-quenching and qI-quenching, for predicting fluorescence fluxes. The novelty and originality of the model lies in the way these fluxes are linked to the state of the photosynthetic apparatus in terms of its photoinhibition level and NPQ activity, a set of conceptual variables that are not accessible via direct measurements.

The remainder of the paper is organized as follows. The principles of fluorescence as well as PAM protocols are briefly discussed in §2. The proposed fluorescence model is presented in §3, including a discussion of its properties. The results of a thorough calibration of the model parameters and its subsequent validation against multiple experimental data sets are reported in §4. Finally, conclusions and a discussion of future research directions are presented in §5.

2. Principles of Chlorophyll Fluorescence

When exposing a photosynthetically active volume to light, a fraction of the light is absorbed by pigment molecules, another fraction is scattered out, and the rest passes through the volume without interaction. In particular, the absorbed photons have three possible fates: they are either captured by the reaction centers of photosystem II (RCII) to drive photosynthesis (photoproduction), dissipated as heat (photoregulation), or re-emitted as fluorescence (Papageorgiou and Govindjee, 2004). Thus, much information about the photosynthetic processes can be inferred by measuring the fluorescence flux under specific lighting protocols that preferentially activate or inactivate the photoproduction and photoregulation mechanisms.

2.1. Pulsed Amplitude Modulation Protocols

PAM fluorometry measures the photosynthetic efficiency of photosystem II in a given sample of microalgae, by using distinct light sources: a weak pulsed measuring light, an actinic light capable of moderate intensities used to drive photosynthesis, and a saturating light of high intensity (Roháček and Barták, 1999; Papageorgiou and Govindjee, 2004). The outcome of a PAM experiment is a record of the fluorescence flux against time, as illustrated in Fig. 1.

Before conducting a PAM experiment, the microalgae sample is kept is the dark during a sufficient long time in order for (i) all RCIIs to be ready to accept electrons (open state), and (ii) NPQ to be inactive—the sample is said to be dark-adapted. At the start of the experiment, the measuring light is switched on to a level weak enough (e.g., $0.1\,\mu\mathrm{E\ m^{-2}\ s^{-1}}$) not to cause significant excitation of the photosynthetic apparatus or trigger NPQ activation—there, the fluorescence detector records the *dark-adapted minimal fluorescence flux*, F_0. Soon after, an intense actinic light pulse is applied (e.g., $6000\,\mu\mathrm{E\ m^{-2}\ s^{-1}}$), and the detector measures the *dark-adapted maximal fluorescence flux*, F_m. The short duration of the pulse (c.a. $1\,\mathrm{s}$) aims to prevent NPQ activation, while triggering complete excitation of all the RCIIs. Next, the actinic light is switched on at a desired irradiance, so the microalgae progressively transit from dark-adapted to light-adapted state as a result of NPQ activation. During this transition, the detector continuously records the *light-adapted realized fluorescence flux*, F', which is decreasing until NPQ has reached a steady state. Every once in a while, a saturating pulse is applied

on top of the actinic light to record the *light-adapted maximal fluorescence flux*, F'_{m}, and the actinic light is also briefly switched off to record the *light-adapted minimal fluorescence flux*, F'_0. After NPQ has reached its steady state, the actinic light is switched off and recording of the realized, maximal and minimal fluorescence fluxes can continue until the microalgae have reverted back to dark-adapted state. Note that the new dark-adapted state at the end of the experiment may be different from the initial dark-adapted state due to the accumulation of damaged RCIIs (Rees et al., 1990).

2.2. Inference of Fluorescence Protocols: Fluorescence Indexes

The main fluorescence *indexes*, also commonly referred to as fluorescence parameters in the literature, are expressed as combinations of the characteristic fluxes F_0, F_{m}, F'_0, F'_{m} and F' described earlier. By discriminating either between dark- and light-adapted states, or between realized, maximal and minimal excitation states, these indexes allow monitoring of specific photosynthetic mechanisms.

The maximum quantum yield of photosynthesis, q, is given by (Kitajima and Butler, 1975):

$$q = \frac{F_{\mathrm{m}} - F_0}{F_{\mathrm{m}}}\,, \tag{1}$$

whereby the difference between F_{m} and F_0 represents the maximum amount of photons that can be used for photoproduction since NPQ is inactive (dark-adapted). In contrast, the realized quantum yield of photosynthesis, Φ_{PS2}, considers light-adapted states:

$$\Phi_{\mathrm{PS2}} = \frac{F'_{\mathrm{m}} - F'}{F'_{\mathrm{m}}}\,, \tag{2}$$

an index also known as the *Genty parameter*, after the researcher who first derived it (Genty et al., 1989). Related indexes include:

$$\Phi_{\mathrm{L}} = \Phi_{\mathrm{PS2}}\frac{F'_0}{F'}\,, \qquad q_{\mathrm{P}} = \frac{F'_{\mathrm{m}} - F'}{F'_{\mathrm{m}} - F'_0}\,, \quad \text{and} \qquad q_{\mathrm{L}} = q_{\mathrm{P}}\frac{F'_0}{F'}\,, \tag{3}$$

with Φ_{L} being useful for monitoring photoinhibition; q_{P} providing a means to quantify the extent of photochemical quenching based on the level of excitation of the photosynthetic apparatus (Bilger and Schreiber, 1987); and q_{L} reflecting the level of interconnectivity in the photosynthetic apparatus

(Kramer et al., 2004). Likewise, the extent of photoregulation can be monitored through the NPQ index, q_{NPQ}, defined as (Bilger and Björkman, 1990):

$$q_{\mathrm{NPQ}} = \frac{F_{\mathrm{m}} - F'_{\mathrm{m}}}{F'_{\mathrm{m}}}\,, \tag{4}$$

whereby the difference between F'_{m} and F_{m} represents the dissipation of energy due to photoregulation.

3. A Dynamic Model of Fluorescence in Microalgae

This section presents a dynamic model of chlorophyll fluorescence that accounts for key photosynthetic processes having time scales up to an hour. Specifically, the model encompasses the processes of photoproduction, photoinhibition and photoregulation, but neglects the changes in photoacclimation state.

In PAM fluorometry, the fluorescence flux F [V] emitted by a microalgae sample of volume V [m^3] and chlorophyll concentration chl [$\mathrm{g(chl)\,m^{-3}}$] can be modeled as (Huot and Babin, 2010):

$$F = I_{\mathrm{m}}\,\sigma\,chl\,\Phi_{\mathrm{f}}\,(1-Q)\,V\,\lambda_{\mathrm{PAM}}\,, \tag{5}$$

where Φ_{f} stands for the quantum yield of fluorescence [$\mu\mathrm{E}\,\mu\mathrm{E}^{-1}$]; σ, the total cross section [$\mathrm{m^2\,g(chl)^{-1}}$]; I_{m}, the measuring light intensity [$\mu\mathrm{E\,m^{-2}\,s^{-1}}$]; Q is a dimensionless parameter describing the percentage of fluorescence absorbed by the sample; and λ_{PAM} [$\mathrm{V\,s\,}\mu\mathrm{E}^{-1}$] is a gain parameter aligning the voltage output of a PAM fluorometer with the actual fluorescence flux. In particular, as chl and Q remain constant for a given photoacclimation state, it is convenient to lump all the constant terms into a single parameter $S_{\mathrm{F}} = I_{\mathrm{m}}\,chl\,(1-Q)\,V\,\lambda_{\mathrm{PAM}}$, giving

$$F = S_{\mathrm{F}}\,\sigma\,\Phi_{\mathrm{f}}\,. \tag{6}$$

In the sequel, we use the Han model to represent the effects of photoproduction and photoinhibition on the fluorescence flux (§3.1) and we develop an extension of that model in order to encompass photoregulation effects (§3.2). Then, we analyze the properties of the resulting model (§3.3).

3.1. Han Model

The model developed by Han (2002) and originating in the works of Kok (1956) and Eilers and Peeters (1988) is based on the concept of photosynthetic unit (PSU), first introduced by Gaffron and Wohl (1936) to represent the physical entity responsible for the production of one O_2 molecule. In this conceptual representation, each PSU is comprised of one RCII and its associated Light Harvesting Complex (LHC), and the chloroplasts are regarded as PSU arrays. Variants of this model have also been developed (Rubio et al., 2003) in order to predict microaglae's photosynthetic activity under varying light conditions.

The description of photoproduction and photoinhibition in the Han model assumes that the RCII of a PSU can be in either one of three states, namely open (A), closed (B) or damaged (C). An RCII in state A is ready to accept an electron; in state B, it is already occupied by electrons; and in state C, it is non-functional. As depicted in Fig. 2, each RCII can transit from one state to another depending on the light irradiance I, with processes described by first-order kinetics. Photoproduction is described by the transition from A to B, while the reverse transition from B to A represents relaxation of the RCII; photoinhibition, on the other hand, corresponds to the transition from B to C, while the reverse transition from C to B describes repair of the damaged RCII by enzymatic processes.

The equations in the Han model describe the dynamics of the fractions of open, closed and damaged RCIIs in the chloroplasts, denoted by $A(t)$, $B(t)$ and $C(t)$, respectively:

$$\dot{A} = -I\,\sigma_{\mathrm{PS2}}\,A + \frac{B}{\tau} \tag{7}$$

$$\dot{B} = I\,\sigma_{\mathrm{PS2}}\,A - \frac{B}{\tau} + k_{\mathrm{r}}\,C - k_{\mathrm{d}}\,\sigma_{\mathrm{PS2}}\,I\,B \tag{8}$$

$$\dot{C} = -k_{\mathrm{r}}\,C + k_{\mathrm{d}}\,\sigma_{\mathrm{PS2}}\,I\,B\,. \tag{9}$$

Here, σ_{PS2} denotes the effective cross section $[\mathrm{m}^2\,\mu\mathrm{E}^{-1}]$; τ, the turnover time $[\mathrm{s}]$; k_{d}, the damage rate constant [–]; and k_{r}, the repair rate constant $[\mathrm{s}^{-1}]$. Moreover, $A(t) + B(t) + C(t) = 1$ at all times.

Several expressions of the fluorescence quantum yield Φ_{f} in (6) as a function of the PSU states A, B and C have been proposed depending on the LHC-RCII configuration. They typically involve the

parameters Φ_{f}^{A}, Φ_{f}^{B} and Φ_{f}^{C} representing the fluorescence quantum yields of an RCII in state A, B or C, respectively (Huot and Babin, 2010). The one configuration used subsequently is the so called Lake Model (Kramer et al., 2004), whereby Φ_{f} is expressed as the harmonic mean of Φ_{f}^{A}, Φ_{f}^{B} and Φ_{f}^{C},

$$\Phi_{\mathrm{f}} = \frac{1}{\frac{A}{\Phi_{\mathrm{f}}^{A}} + \frac{B}{\Phi_{\mathrm{f}}^{B}} + \frac{C}{\Phi_{\mathrm{f}}^{C}}} \,. \tag{10}$$

In analogy to parallel electrical circuits, this configuration assumes that all RCIIs are connected to a common LHC and thus compete for the incoming excitation energy. Naturally, other types of LHC-RCII configurations can be used in the fluorescence model if desired.

Besides Φ_{f}, the total cross-section σ in (6) can be related to the parameter σ_{PS2} in the Han model. In a first step, σ is related to the so-called optical cross section, σ_{PSU} $[\mathrm{m}^2\,\mu\mathrm{mol}(\mathrm{O_2})^{-1}]$, as

$$\sigma = \sigma_{\mathrm{PSU}}\, N \,, \tag{11}$$

with N the number of PSUs $[\mu\mathrm{mol}(\mathrm{O_2})\,\mathrm{g}(\mathrm{chl})^{-1}]$, which remains constant for a given photoacclimation state. In a second step, σ_{PS2} can be related to σ_{PSU} as (Falkowski and Raven, 1997)

$$\sigma_{\mathrm{PS2}} = \nu\, \Phi_{\mathrm{p}}^{A}\, \sigma_{\mathrm{PSU}} \,, \tag{12}$$

where Φ_{p}^{A} $[\mu\mathrm{E}\,\mu\mathrm{E}^{-1}]$ denotes the quantum yield of photosynthesis of an open RCII, which is equal to the realized quantum yield of photosynthesis Φ_{PS2} in the case that $A = 1$ (see §3.3 for an expression of Φ_{p}^{A}); and $\nu = 4\,\mu\mathrm{E}\,\mu\mathrm{mol}(\mathrm{O_2})^{-1}$ is a conversion factor reflecting the minimum theoretical (minimal) value of 4 electrons produced for each molecule of water dissociated.

3.2. Accounting for Photoregulation

An important limitation of the Han model in the context of PAM fluorometry is that some of its parameters may vary on the time scale of minutes due to certain NPQ regulation mechanisms being activated. Two types of NPQ mechanisms are accounted for in this work, namely qI-quenching and qE-quenching, which are often seen as the major contributors to fluorescence quenching on the time

scales of interest (Horton and Hague, 1988). qE-quenching is activated at high light irradiance by low thylakoid lumenal pH (Bilger and Björkman, 1990); it evolves within minutes and can result in up to 90% reduction in fluorescence (Huot and Babin, 2010). qI-quenching is linked to photoinhibition, according to the biological hypothesis that damaged RCII can trap and dissipate excited electrons as heat; it typically evolves in a time scale of minutes to hours and can be responsible for up to 40% reduction in fluorescence (Falkowski et al., 1993).

We start by noting that only qE-quenching requires further consideration as qI-quenching is already accounted for through the dependence of Φ_{f} on the fraction C of damaged RCIIs in (10). Since qE-quenching in the dark is negligible and varies with the light irradiance via the change in lumenal pH, we introduce a conceptual qE-activity reference function α_{ss} taking values in the range $[0, 1]$ and increasing with I, from the level $\alpha_{\mathrm{ss}} = 0$ at $I = 0$. After consideration of experimental measurements of the NPQ index (4) as a function of I (Kramer et al., 2004), we choose to formulate α_{ss} as a sigmoid (Hill) function of I:

$$\alpha_{\mathrm{ss}}(I) = \frac{I^n}{I_{\mathrm{qE}}^n + I^n}\,, \tag{13}$$

where I_{qE} [$\mu\mathrm{E}^{-1}$] represents the irradiance level at which half of the maximal qE-activity is realized ($\alpha_{\mathrm{ss}} = 0.5$); and n [–] describes the sharpness of the transition, approaching switch-like behavior as n becomes larger. In addition, we describe tracking of the qE-activity reference α_{ss} by the actual qE-activity level $\alpha(t)$ as a first-order process:

$$\dot{\alpha} = \xi\,(\alpha_{\mathrm{ss}}(I) - \alpha)\,, \tag{14}$$

where ξ [s^{-1}] denotes the rate of NPQ adaptation, which shall be assumed constant here on the time scales of interest.

In accounting for the effect of qE-activity α on the fluorescence flux F in (6), both Φ_{f} and σ could, in principle, depend on α, and possibly simultaneously. After consideration of multiple experimental data sets and model variants, and in an objective to minimize the number of assumptions and model parameters, we choose to express the dependence on Φ_{f} only—we shall come back to this important point later on in the results section. Following Kitajima and Butler (1975); Oxborough and Baker

(1997) and Huot and Babin (2010), we express the fluorescence quantum yields as

$$\Phi_{\mathrm{f}}^{A} = \frac{1}{1+\eta_{\mathrm{P}}+\eta_{\mathrm{D}}+\eta_{\mathrm{qE}}}\,, \qquad \Phi_{\mathrm{f}}^{B} = \frac{1}{1+\eta_{\mathrm{D}}+\eta_{\mathrm{qE}}}\,, \qquad \Phi_{\mathrm{f}}^{C} = \frac{1}{1+\eta_{\mathrm{I}}+\eta_{\mathrm{D}}+\eta_{\mathrm{qE}}}\,, \tag{15}$$

where the parameters η_{P}, η_{D}, η_{qE} and η_{I} represent, respectively, the rates of photoproduction, basal thermal decay in dark-adapted state, qE-quenching and qI-quenching, all relative to the rate of fluorescence; that is, these four parameters are dimensionless. Observe that Φ_{f}^{B} does not depend on η_{P} as a closed RCII cannot support photoproduction, and Φ_{f}^{C} depends on η_{I} instead of η_{P} in order to account for the effect of qI-quenching. Moreover, following Oxborough and Baker (2000), we capture the effect of qE-quenching by expressing η_{qE} as a linear relationship of the qE-activity level α:

$$\eta_{qE} = \overline{\eta}_{\mathrm{qE}}\,\alpha\,, \tag{16}$$

with $\overline{\eta}_{\mathrm{qE}}$ a parameter describing the maximum rate of energy dissipation. Finally, an expression of the fluorescence flux F is obtained by substituting (15) and (16) back into (6), giving

$$F = \frac{S_{\mathrm{F}}\sigma}{1+\eta_{\mathrm{D}}+\overline{\eta}_{\mathrm{qE}}\,\alpha + A\,\eta_{\mathrm{P}} + C\,\eta_{\mathrm{I}}}\,. \tag{17}$$

3.3. Properties of Fluorescence Model

In PAM fluorometry, the fluorescence flux F in (17) corresponds to the light-adapted realized fluorescence flux F'—see §2.1. The remaining characteristic fluorescence fluxes F_0, F_{m}, F_0' and F_{m}' are obtained by specializing (17) with $A = 0$ and $B = 0$ for the maximal and minimal fluorescence fluxes, respectively, and with $\alpha = 0$ for the dark-adapted fluorescence fluxes. These expressions are reported in the left part of Table I.

Mathematical expressions of the fluorescence indexes discussed in §2.2 follow readily from substitution of the foregoing PAM flux expressions. Two sets of expressions are reported in the right part of Table I, corresponding to whether or not the assumption $\Phi_{\mathrm{f}}^{A} = \Phi_{\mathrm{f}}^{C}$ is made—or, equivalently, $\eta_{\mathrm{I}} = \eta_{\mathrm{P}}$. This assumption originates in the work of Maxwell and Johnson (2000), who argued that quenching related to RCII damage does not cause a variation in the light-adapted minimal fluorescence flux F_0',

thus implying that the fraction of incoming photons leading to photoproduction in an open RCII should be the same as the fraction of incoming photons dissipated as heat in a damaged RCII.

A number of comments are in order regarding the fluorescence index expressions:

- The realized quantum yield of photosynthesis, Φ_{PS2}, turns out to be a nonlinear function of the open, closed and damaged RCII fractions, irrespective of the assumption $\Phi_{\mathrm{f}}^{A} = \Phi_{\mathrm{f}}^{C}$. This result suggests that the usual hypothesis of a linear relationship between Φ_{PS2} and the fraction A of open RCIIs could be inaccurate, especially when the fraction B of closed RCIIs is small. An expression of the quantum yield of photosynthesis of an open RCII, defined as Φ_{p}^{A} earlier in (12), can also be derived from the expression of Φ_{PS2} in the special case that $A = 1$:

$$\Phi_{\mathrm{p}}^{A} = \frac{\eta_{\mathrm{P}}}{1 + \eta_{\mathrm{D}} + \overline{\eta}_{\mathrm{qE}}\alpha + \eta_{\mathrm{P}}} \,. \tag{18}$$

- The maximum quantum yield of photosynthesis, q, is a nonlinear function of the fraction C of damaged RCIIs in the dark-adapted sample in general, but this dependency becomes linear under the assumption that $\Phi_{\mathrm{f}}^{A} = \Phi_{\mathrm{f}}^{C}$.

- The photochemical quenching index, q_{L}, is found to be equal to the ratio of open-to-active RCIIs, which is in agreement with the considerations in Kramer et al. (2004).

Finally, we note that an expression of the fraction C of damaged RCIIs can be obtained as a function of the fluorescence indexes Φ_{L} and q_{L} in the form:

$$C = 1 - \frac{\Phi_{\mathrm{L}}(1 + \eta_{\mathrm{D}} + \overline{\eta}_{\mathrm{qE}}\alpha + \eta_{\mathrm{I}})}{\Phi_{\mathrm{L}}(\eta_{\mathrm{I}} - \eta_{\mathrm{P}}) + q_{\mathrm{L}}\eta_{\mathrm{P}}} \,. \tag{19}$$

A detailed derivation of this expression is reported in Appendix A. This relation is particularly useful from a practical standpoint as it allows predicting the level of damage of the photosynthetic apparatus based on experimental measurements of Φ_{L} and q_{L}, in combination with the qE-activity level α predicted by (13)-(14). In particular, the latter equations are independent of the states of the PSUs due to the cascade structure of the fluorescence model. Similar expressions can be obtained for the fractions A and B of open/closed RCIIs by noting that $A = (1 - C)q_{\mathrm{L}}$ and $B = (1 - C)(1 - q_{\mathrm{L}})$.

4. Results and Discussion

This section presents the calibration results of the chlorophyll fluorescence model developed in §3 together with a validation analysis. ~~The experimental data are obtained using PAM fluorometry for the microalga *Nannochloropsis gaditana*, and different data sets are considered for the purposes of calibration and validation. All the dynamic simulations and parameter estimation problems are carried out in the modelling environment gPROMS (`http://www.psenterprise.com`).~~

4.1. Material and Methods

The microalga *Nannochloropsis gaditana* (CCAP, strain 849/5) was grown in a sterile, filtered F/2 medium, using sea salts (32 $\mathrm{g/L}$) from Sigma, 40 $\mathrm{mM Tris}$ HCl, pH 8 and Sigma Guillard's (F/2) marine water enrichment solution. Growth experiments were conducted in the multi-cultivator MC 1000-OD system (Photon Systems Instruments, Czech Republic), with daily measurements of the growth rate via changes in optical density OD 720 using spectrosphotometry. The suspension culture was continuously mixed and aerated by bubbling air, maintained at a temperature of $21\,^{\circ}\mathrm{C}$, and subject to a constant light intensity of 100 $\mu\mathrm{E\,m^{-2}\,s^{-1}}$ supplied by an array of white LEDs. Samples were harvested from the multicultivator after 5 days (late exponential phase), so that the microalgae are acclimated to these conditions, yet still actively growing and not experiencing nutrients depletion. A pre-culture was also grown at 100 $\mu\mathrm{E\,m^{-2}\,s^{-1}}$ in glass bottles of 0.25 L under a continuous airflow, enriched with 5% CO_2. At the exponential growth phase, this pre-culture was centrifuged and re-suspended in fresh medium to reach a final concentration of 9×10^6 cells/ml, before its introduction in the multi-cultivator.

All the fluorescence measurements were performed using a Dual PAM (Walz, Germany), after a dark adaptation period of 20 minutes, by exposing the microalgae samples to variable actinic light intensities in time intervals of 60 seconds. Before switching-on of the actinic light and during the final 2 s of each interval, a saturating light pulse at 6000 $\mu\mathrm{E\,m^{-2}\,s^{-1}}$ was applied during 0.6 s, followed by a dark period (actinic light off) of 1.4 s; measurements were recorded before and after the saturating pulses and after the dark periods, which correspond to F', F'_{m} and F'_0, respectively.

Two separate experiments were performed for the purpose of model calibration (§4.2) and validation (§4.3). Both light protocols are reported, with the corresponding fluorescence flux data, in Appendix

B. The simulations of the fluorescence model were conducted in the modeling environment gPROMS[1]. The calibration too was performed in gPROMS using maximum likelihood estimation and statistical confidence analysis (Walter and Pronzato, 1997), in order for the model predictions to match the measured fluorescence fluxes F', F'_{m} and F'_0. Due to lack of further information regarding the precision and accuracy of the PAM fluorometer, a 1% standard deviation was assumed for the measured fluorescence fluxes to determine the parameters and estimate their confidence intervals.

4.2. Model Calibration

The chlorophyll fluorescence model developed in §3 comprises a total of 13 parameters, many of which have unknown values and thus need to be estimated. The light protocol and fluorescence flux measurements used for purpose of model calibration are shown on Fig. 3 (gray-shaded area and points with error bars, respectively). The first part of the experiment shows a gradual increase of the actinic light intensity from 0 to 1960 $\mu\mathrm{E\,m^{-2}\,s^{-1}}$ in stages of 60 s, before the switching-off of the actinic light around 1000 s until the final time of 1200 s. The corresponding data can be found in Tables III and IV (Appendix B).

Not all 13 parameter values can be estimated with high confidence from this data set, as certain parameters are insensitive or turn out to be highly correlated, if at all identifiable. Model reduction techniques could be used in order to arrive at a simpler model, but this would entail loss of physical meaning for (part of) the states and/or parameters and so was not considered here. After solving multiple instances of the parameter estimation problem for various subsets of parameters, we found that 9 parameters can be confidently estimated by keeping the following 4 parameters τ, k_{r}, N and η_{D} constant:

- The parameter τ representing relaxation of the closed RCIIs in the Han model, a process acting on very fast time scales, turns out to have a very small effect on the predicted fluxes. On the other hand, the parameter k_{r} describing repair of the damaged RCIIs on a time scale of hours cannot be confidently estimated from experimental data collected over 20 minutes only. The values for τ and k_{r} in Table II are the mean values of the ranges reported by Han et al. (2000). One way

[1]Process Systems Enterprise, gPROMS, `www.psenterprise.com/gproms`, 1997-2014

of determining τ experimentally would be to use fast repetition rate (FFR) fluorometry that can apply flashes at microsecond intervals (Kolber et al., 1998). Likewise, a more confident estimate for k_r could be obtained by simply extending the dark phase at the end of the calibration PAM experiment, e.g., by an hour or two.

- The total number of PSUs, N, cannot be confidently estimated due to its large correlation with the total cross-section σ ~~when using fluorescence data collected over short time periods~~. The value for N in Table II is based on the Emerson number of 2,500 $\mathrm{mol(chl)\,mol(O_2)^{-1}}$, as reported by Falkowski and Raven (1997).

- The parameter subset formed by the relative rate constants η_{P}, η_{D}, $\overline{\eta}_{\mathrm{qE}}$, η_{I} and the scaling factor S_{f} in (17) is structurally unidentifiable based on fluorescence flux measurements only, calling for fixing the value of one of these parameters. The parameter η_{D} representing the rate of basal thermal decay relative to the rate of fluorescence can be estimated based on the probability of thermal dissipation and the probability of fluorescence for a photon absorbed by a dark adapted RCII. The value in Table II is the mean of those η_{D} values for which the resulting fluorescence quantum yields are consistent with the data by Huot and Babin (2010).

The parameter values and 95% confidence intervals determined by gPROMS using maximum-likelihood estimation are reported in the right part of Table II. The corresponding fits of F', F'_{m} and F'_0 against the measured fluxes are shown in Fig. 3, both without and with the assumption $\Phi_{\mathrm{f}}^A = \Phi_{\mathrm{f}}^C$. Note that the predicted fluorescence fluxes are in excellent agreement with the measured fluxes, thereby providing a first confirmation that the proposed model structure captures the interplay between photoproduction, photoinhibition and photoregulation in a typical PAM experiment. Moreover, all the parameter estimates, but k_{d} and η_{I}, have 95% confidence interval below 10%, which is quite remarkable given the large number of estimated parameters and the apparent simplicity of the PAM protocol in Fig. 3. Although the estimated values of k_{d} and η_{I} are found to pass the statistical t-test, the presence of a large correlation between these parameters explains their relatively poor precision. Under the assumption that $\Phi_{\mathrm{f}}^A = \Phi_{\mathrm{f}}^C$, or equivalently $\eta_{\mathrm{I}} = \eta_{\mathrm{P}}$, the 95% confidence intervals are reduced under 10%, without significantly affecting the rest of the parameters. Nonetheless this assumption would require

further testing and validation before adoption.

4.3. Model Analysis and Validation

Besides predicting the fluorescence fluxes well, the ability of the model to predict the fluorescence indexes q_{L}, Φ_{PS2} and q_{NPQ} is depicted in Fig. 4, based on the expressions given in the right part of Table I. The index Φ_{PS2} is predicted quite accurately by the model throughout the entire time horizon, and the smooth transition in the Φ_{PS2} profile observed once the actinic light is switched off is a consequence of qE-quenching acting directly on the quantum yield of photosynthesis in the proposed NPQ representation. Moreover, the predicted value of 0.65 for the quantum yield of photosynthesis of a dark-adapted open RCII—this value corresponds to the Φ_{PS2} at initial time here—is in excellent agreement with values widely reported in the literature (Sforza et al., 2012; Simionato et al., 2011; Kolber and Falkowski, 1993). The overall fitting quality of the index q_{L} is also satisfactory, apart from the last few experimental points during the light phase (between 800-1000 s), which are over-predicted by the model. Nonetheless, the model captures well the sharp change in q_{L} that occurs when the actinic light is switched off, a property that comes forward with the expression of q_{L} in Table I due to the fast dynamics of A and B. Finally, the accurate predictions of q_{NPQ} in the lower plot of Fig. 4 provide another confirmation that the NPQ regulation is captured adequately by the selected model structure.

Further validation of the model can be obtained upon analyzing the level of photoinhibition created by the continuously increasing actinic light. Specifically, the main plot on Fig. 5 shows a comparison between the fraction C of damaged RCIIs predicted by the full calibrated model and the same fraction given by (19). We recall that the later uses the available fluorescence flux measurements in combination with the predicted qE-activity level α, but does not rely on the Han model at all. These two damage fractions are found to be in good agreement, especially when considering the error bars and the red envelope of predictions computed from the 95% confidence intervals of the calibrated parameters in both cases. These rather large errors—between 0.02-0.07 at the end of the light phase—are caused by the rather large confidence intervals for the parameters k_{d} and η_{I} in this case. For comparison purposes, the smaller plot on Fig. 5 shows the predictions of an alternative model of qE-quenching, whereby the qE-activity variable α modifies the absorption cross section σ in (5) instead of the quantum yield of fluorescence Φ_{f}. As well as the large discrepancy between both predictions of the damage level, it is

the unusually large damage level (up to 60% after 1000 s) along with the fast repair rate that clearly invalidate this alternative qE-quenching representation.

The foregoing results suggest that the proposed fluorescence model is capable of quantitative predictions of the state of the photosynthetic apparatus under varying light conditions. To confirm it, we carry out a validation experiment for an (unusually) challenging PAM experiment, as shown in gray-shaded area on Fig. 6. The corresponding model predictions, based on the default and calibrated model parameters in Table II, are compared to the actual flux measurements in Fig. 6. Although calibrated for a quite different and somewhat simpler PAM protocol, the calibrated model remains capable of reliable quantitative predictions of the fluorescence fluxes. Deviations are observed in various parts of the response flux profiles, which are possibly due to effects and processes not accounted for in the proposed model, yet these deviation remain small, within 10-20%. We also note that such extreme variations of the light conditions, however useful in a model validation context, are unlikely to be found in a practical microalgae culture systems.

5. Conclusions

This paper proposes a mathematical representation of key photosynthetic processes acting on time scales up to an hour and triggered by varying light conditions, which are typical in PAM experiments. The dynamic fluorescence model relies on the combination of fast photosynthetic mechanisms with slower photoprotective mechanisms in order to yield a light-dependent expression of the quantum yield of photosynthesis. Despite comprising a total of 13 parameters, a careful calibration and subsequent validation against multiple experimental data sets shows that the model is capable of quantitative predictions of the state of the photosynthetic apparatus in terms of its open, closed and damaged reaction center. This makes it the first model of its kind capable of reliable predictions of the levels of photoinhibition and NPQ activity, while retaining a low complexity and a small dimensionality.

Such generic capability to predict the development of photoinhibition and photoregulation, yet without the need for dedicated experiments (Ruban and Murchie, 2012), addresses a long-standing challenge in the modelling of photosynthetic productivity and holds much promise in regard of future applications. By design, the fluorescence model is indeed capable of simulating experimental protocols

used for the determination of PI-response curves, yet avoiding the usual—and somewhat problematic—static growth assumption. One can for instance consider the following expression of the photosynthesis rate P as

$$P = I\sigma\Phi\,, \tag{20}$$

where Φ is the photosynthesis quantum yield, which is closely related to the quantum yield of the ETR, Φ_{PS2}, and can be measured by PAM fluorometry (Suggett et al., 2003). This opens the possibility for a cross-validation framework, whereby both fluorescence and classical growth experiments could be used for model validation purposes. In combination with dedicated PAM experiments, there is also hope that the model could serve as a platform for unveiling previously hidden information concerning the operation of the photosynthetic apparatus. Because PAM experiments are both precise and fast, a full validation of the model appears tractable in this context, especially if model-based experimental design is used for testing the model structure further, e.g., through the determination of information-rich PAM protocols.

Incorporating photoacclimation processes is currently investigated as part of future work in order to widen the applicability of the model, such as predicting the evolution of a microalgae culture over time periods of several days or even weeks. Eventually, the vision is to integrate a fully validated model of photosynthesis within first-principle models describing the flow and light attenuation in large-scale microalgae culture systems as a means to guide their design and operations.

Acknowledgment. AN and BC gratefully acknowledge financial support by ERC career integration grant PCIG09-GA-2011-293953 (DOP-ECOS). TM gratefully acknowledges financial support by ERC starting grant 309485 (BIOLEAP). AB and FB gratefully acknowledge Fondazione Cariparo for grant Progetto Dottorati di Ricerca 2012.

References

Baker, N. R., 2008. Chlorophyll fluorescence: A probe of photosynthesis in vivo. Annual Review of Plant Biology 59 (1), 89–113.

Bilger, W., Björkman, O., 1990. Role of the xanthophyll cycle in photoprotection elucidated by measurements of light-induced absorbance changes, fluorescence and photosynthesis in leaves of hedera canariensis. Photosynthesis Research 25 (3), 173–185.

Bilger, W., Schreiber, U., 1987. Energy-dependent quenching of dark-level chlorophyll fluorescence in intact leaves. In: Excitation Energy and Electron Transfer in Photosynthesis. Springer, pp. 157–162.

Chisti, Y., 2007. Biodiesel from microalgae. Biotechnology Advances 25 (3), 294–306.

Cornet, J. F., Dussap, C. G., Cluzel, P., Dubertret, G., 1992. A structured model for simulation of cultures of the cyanobacterium *Spirulina platensis* in photobioreactors: II. Identification of kinetic parameters under light and mineral limitations. Biotechnology & Bioengineering 40 (7), 826–834.

Eilers, P. H. C., Peeters, J. C. H., 1988. A model for the relationship between light intensity and the rate of photosynthesis in phytoplankton. Ecological Modelling 42 (3), 199–215.

Falkowski, P. G., Greene, R., Kolber, Z. S., 1993. Light utilization and photoinhibition of photosynthesis in marine phytoplankton. Tech. rep., Brookhaven National Laboratory, Upton (NY).

Falkowski, P. G., Raven, J. A., 1997. Aquatic photosynthesis. Vol. 256. Blackwell Science Malden, MA.

Gaffron, H., Wohl, K., 1936. Zur theorie der assimilation. Naturwissenschaften 24 (6), 81–90.

Genty, B., Briantais, J.-M., Baker, N. R., 1989. The relationship between the quantum yield of photosynthetic electron transport and quenching of chlorophyll fluorescence. Biochimica et Biophysica Acta (BBA) - General Subjects 990 (1), 87 – 92.

Han, B. P., 2002. A mechanistic model of algal photoinhibition induced by photodamage to photosystem-II. Journal of Theoretical Biology 214 (4), 519–27.

Han, B.-P., Virtanen, M., Koponen, J., Straškraba, M., 2000. Effect of photoinhibition on algal photosynthesis: a dynamic model. Journal of Plankton Research 22 (5), 865–885.

Horton, P., Hague, A., 1988. Studies on the induction of chlorophyll fluorescence in isolated barley protoplasts. iv. resolution of non-photochemical quenching. Biochimica et Biophysica Acta (BBA)-Bioenergetics 932, 107–115.

Huot, Y., Babin, M., 2010. Overview of fluorescence protocols: theory, basic concepts, and practice. In: Chlorophyll a Fluorescence in Aquatic Sciences: Methods and Applications. Springer, pp. 31–74.

Kitajima, M., Butler, W. L., 1975. Quenching of chlorophyll fluorescence and primary photochemistry in chloroplasts by dibromothymoquinone. Biochimica et Biophysica Acta (BBA)-Bioenergetics 376 (1), 105–115.

Kok, B., 1956. On the inhibition of photosynthesis by intense light. Biochimica et Biophysica Acta 21 (2), 234–244.

Kolber, Z. S., Falkowski, P. G., 1993. Use of active fluorescence to estimate phytoplankton photosynthesis in situ. Limnology & Oceanography 38 (8), 1646–1665.

Kolber, Z. S., Pràšil, O., Falkowski, P. G., 1998. Measurements of variable chlorophyll fluorescence using fast repetition rate techniques: defining methodology and experimental protocols. Biochimica et Biophysica Acta (BBA) - Bioenergetics 1367 (1-3), 88–106.

Kramer, D. M., Johnson, G., Kiirats, O., Edwards, G. E., 2004. New fluorescence parameters for the determination of q(a) redox state and excitation energy fluxes. Photosynthesis Research 79 (2), 1209–218.

Long, S. P., Humphries, S., Falkowski, P. G., 1994. Photoinhibition of photosynthesis in nature. Annual Review of Plant Physiology & Plant Molecular Biology 45 (1), 633–662.

MacIntyre, H. L., Kana, T. M., Anning, T., Geider, R. J., 2002. Photoacclimation of photosynthesis irradiance response curves and photosynthetic pigments in microalgae and cyanobacteria1. Journal of Phycology 38 (1), 17–38.

Maxwell, K., Johnson, G. N., 2000. Chlorophyll fluorescence - a practical guide. Journal of Experimental Botany 51 (345), 659–668.

Müller, P., Li, X.-P., Niyogi, K. K., 2001. Non-photochemical quenching. a response to excess light energy. Plant Physiology 125 (4), 1558–1566.

Mutanda, T., Ramesh, D., Karthikeyan, S., Kumari, S., Anandraj, A., Bux, F., 2011. Bioprospecting for hyper-lipid producing microalgal strains for sustainable biofuel production. Bioresource Technology 102 (1), 57–70.

Oxborough, K., Baker, N. R., 1997. Resolving chlorophyll a fluorescence images of photosynthetic efficiency into photochemical and non-photochemical components – calculation of qP and Fv'/Fm' without measuring Fo'. Photosynthesis Research 54 (2), 135–142.

Oxborough, K., Baker, N. R., 2000. An evaluation of the potential triggers of photoinactivation of photosystem II in the context of a Stern-Volmer model for downregulation and the reversible radical pair equilibrium model. Philosophical Transactions of the Royal Society of London. Series B: Biological Sciences 355 (1402), 1489–1498.

Papageorgiou, G. C., Govindjee, 2004. Chlorophyll a Fluorescence: A Signature of Photosynthesis. Vol. 19. Springer, Dordrecht, The Netherlands.

Rees, D., Noctor, G. D., Horton, P., 1990. The effect of high-energy-state excitation quenching on maximum and dark level chlorophyll fluorescence yield. Photosynthesis Research 25 (3), 199–211.

Roháček, K., 2002. Chlorophyll fluorescence parameters: the definitions, photosynthetic meaning, and mutual relationships. Photosynthetica 40 (1), 13–29.

Roháček, K., Barták, M., 1999. Technique of the modulated chlorophyll fluorescence: basic concepts, useful parameters, and some applications. Photosynthetica 37 (3), 339–363.

Ruban, A. V., Murchie, E. H., 2012. Assessing the photoprotective effectiveness of non-photochemical chlorophyll fluorescence quenching: A new approach. Biochimica et Biophysica Acta (BBA)-Bioenergetics 1817 (7), 977–982.

514 Rubio, F. C., Camacho, F. G., Sevilla, J. M., Chisti, Y., Grima, E. M., 2003. A mechanistic model of
515 photosynthesis in microalgae. Biotechnology & Bioengineering 81 (4), 459–473.

516 Sforza, E., Simionato, D., Giacometti, G. M., Bertucco, A., Morosinotto, T., 2012. Adjusted light and
517 dark cycles can optimize photosynthetic efficiency in algae growing in photobioreactors. PloS One
518 7 (6), e38975.

519 Sheehan, J., Dunahay, T., Benemann, J., Roessler, P., 1998. A Look Back at the U.S. Department of
520 Energy's Aquatic Species Program – Biodiesel from Algae. Tech. rep., U.S. Department of Energy.

521 Simionato, D., Sforza, E., Corteggiani Carpinelli, E., Bertucco, A., Giacometti, G. M., Morosinotto, T.,
522 2011. Acclimation of *Nannochloropsis gaditana* to different illumination regimes: Effects on lipids
523 accumulation. Bioresource Technology 102 (10), 6026–6032.

524 Suggett, D. J., Oxborough, K., Baker, N. R., MacIntyre, H. L., Kana, T. M., Geider, R. J., 2003. Fast
525 repetition rate and pulse amplitude modulation chlorophyll a fluorescence measurements for assess-
526 ment of photosynthetic electron transport in marine phytoplankton. European Journal of Phycology
527 38 (4), 371–384.

528 Walter, E., Pronzato, L., 1997. Identification of Parametric Models from Experimental Data. Commu-
529 nications and Control Engineering. Springer, New York.

530 Williams, P. J. l. B., Laurens, L. M. L., 2010. Microalgae as biodiesel & biomass feedstocks: Review
531 & analysis of the biochemistry, energetics & economics. Energy & Environmental Science 3 (5),
532 554–590.

533 Appendix A. Derivation of Mathematical Expression of Damaged Reaction Centers

Starting with the expression of the fluorescence index q_L in Table I,

$$q_{\mathrm{L}} = \frac{A}{A+B}\,,$$

and using the property $A + B + C = 1$, we obtain

$$C = 1 - \frac{A}{q_{\mathrm{L}}} \,. \tag{A.1}$$

Then, from the expression of the fluorescence index Φ_{L} also in Table I,

$$\Phi_{\mathrm{L}} = \frac{A\eta_{\mathrm{P}}}{1 + \eta_{\mathrm{D}} + \overline{\eta}_{\mathrm{qE}}\alpha + (1 - C)\eta_{\mathrm{P}} + C\eta_{\mathrm{I}}} \,,$$

we can express the fraction of open reaction centers A as

$$A = \frac{\Phi_{\mathrm{L}}(1 + \eta_{\mathrm{D}} + \overline{\eta}_{\mathrm{qE}}\alpha + (1 - C)\eta_{\mathrm{P}} + C\eta_{\mathrm{I}})}{\eta_{\mathrm{P}}} \,. \tag{A.2}$$

Expression (19) of the fraction of damaged reaction centers C as a function of the qE-activity level α follows by substituting (A.2) into (A.1) and simple algebraic manipulations.

Appendix B. Calibration and Validation Data Sets

For completeness and reproducibility of our results, we report the light protocols (Table III) and the corresponding fluorescence measurements (Table IV) for both calibration and validation data sets.

List of Tables

Table I: Expressions of PAM fluorescence fluxes (left side) and fluorescence indexes (right side).

Flux	Expression
F'	$\dfrac{S_\mathrm{F}\sigma}{1+\eta_\mathrm{D}+\overline{\eta}_\mathrm{qE}\alpha+A\eta_\mathrm{P}+C\eta_\mathrm{I}}$
F'_m	$\dfrac{S_\mathrm{F}\sigma}{1+\eta_\mathrm{D}+\overline{\eta}_\mathrm{qE}\alpha+C\eta_\mathrm{I}}$
F'_0	$\dfrac{S_\mathrm{F}\sigma}{1+\eta_\mathrm{D}+\overline{\eta}_\mathrm{qE}\alpha+(1-C)\eta_\mathrm{P}+C\eta_\mathrm{I}}$
F_m	$\dfrac{S_\mathrm{F}\sigma}{1+\eta_\mathrm{D}+C\eta_\mathrm{I}}$
F_0	$\dfrac{S_\mathrm{F}\sigma}{1+\eta_\mathrm{D}+(1-C)\eta_\mathrm{P}+C\eta_\mathrm{I}}$

Index	$\eta_\mathrm{P}\neq\eta_\mathrm{I}$	$\eta_\mathrm{P}=\eta_\mathrm{I}$
Φ_PS2	$\dfrac{A\eta_\mathrm{P}}{1+\eta_\mathrm{D}+\overline{\eta}_\mathrm{qE}\alpha+A\eta_\mathrm{P}+C\eta_\mathrm{I}}$	$\dfrac{A\eta_\mathrm{P}}{1+\eta_\mathrm{D}+\overline{\eta}_\mathrm{qE}\alpha+(1-B)\eta_\mathrm{P}}$
q	$\dfrac{(1-C)\eta_\mathrm{P}}{1+\eta_\mathrm{D}+(1-C)\eta_\mathrm{P}+C\eta_\mathrm{I}}$	$\dfrac{(1-C)\eta_\mathrm{P}}{1+\eta_\mathrm{D}+\eta_\mathrm{P}}$
q_L	$\dfrac{A}{A+B}$	$\dfrac{A}{A+B}$

Table II: Default values of the constant parameters (left part), and estimated values with confidence intervals of the calibrated parameters (right part).

Parameter	Value	Units
k_{r}	5.55×10^{-5}	s^{-1}
τ	5.50×10^{-3}	s
N	4.48×10^{-1}	$\mu\mathrm{mol(O_2)\ g(chl)}^{-1}$
η_{D}	5.00×10^{0}	-

Parameter	Estimate	$\pm 95\%$ Conf. Int.	Units
ξ	5.95×10^{-2}	$\pm 6.65 \times 10^{-3}$	s^{-1}
n	2.26×10^{0}	$\pm 7.76 \times 10^{-2}$	s^{-1}
I_{qE}	8.56×10^{2}	$\pm 2.88 \times 10^{1}$	$\mu\mathrm{E\ m}^{-2}\ \mathrm{s}^{-1}$
k_{d}	6.41×10^{-7}	$\pm 3.38 \times 10^{-7}$	-
η_{P}	1.14×10^{1}	$\pm 1.60 \times 10^{-1}$	-
η_{I}	7.87×10^{1}	$\pm 3.94 \times 10^{1}$	-
$\overline{\eta}_{\mathrm{qE}}$	1.98×10^{1}	$\pm 6.69 \times 10^{-1}$	-
σ	1.75×10^{0}	$\pm 8.70 \times 10^{-2}$	$\mathrm{m}^2 \mu\mathrm{E}^{-1}$
S_{f}	7.79×10^{-1}	$\pm 3.90 \times 10^{-2}$	$\mathrm{g(chl)}\ \mu\mathrm{E}^{-1}\ \mathrm{V}^{-1}$

Table III: PAM actinic light profiles for the calibration and validation experiments.

Step	Duration [sec]	Calibration Irradiance [μE $\mathrm{m}^{-2}\mathrm{s}^{-1}$]	Validation Irradiance [μE $\mathrm{m}^{-2}\mathrm{s}^{-1}$]
1	60	14	14
2	60	21	21
3	60	45	1602
4	60	78	1960
5	60	134	45
6	60	174	78
7	60	224	1036
8	60	281	1295
9	60	347	134
10	60	438	174
11	60	539	1602
12	60	668	1960
13	60	833	45
14	60	1036	78
15	60	1602	134
16	60	1602	1960
17	60	1960	1960
18	60	14	0
19	60	14	0
20	60	14	0

Table IV: Fluorescence flux measurements for the calibration and validation experiments.

	Calibration			Validation		
Time [sec]	F' [V]	F'_{m} [V]	F'_0 [V]	F' [V]	F'_{m} [V]	F'_0 [V]
0	0.077	0.223	0.078	0.090	0.221	0.090
60	0.083	0.224	0.078	0.094	0.222	0.090
120	0.082	0.227	0.078	0.094	0.225	0.091
180	0.083	0.226	0.078	0.064	0.067	0.047
240	0.084	0.222	0.078	0.053	0.055	0.040
300	0.087	0.214	0.077	0.087	0.161	0.078
360	0.088	0.209	0.076	0.090	0.174	0.081
420	0.088	0.198	0.075	0.051	0.057	0.041
480	0.087	0.180	0.072	0.046	0.049	0.037
540	0.083	0.160	0.069	0.079	0.136	0.072
600	0.079	0.137	0.064	0.080	0.135	0.071
660	0.073	0.116	0.059	0.048	0.050	0.038
720	0.067	0.098	0.054	0.042	0.043	0.033
780	0.061	0.082	0.049	0.075	0.127	0.069
840	0.057	0.070	0.044	0.082	0.142	0.073
900	0.053	0.061	0.041	0.080	0.137	0.072
960	0.050	0.055	0.038	0.047	0.048	0.036
1020	0.047	0.051	0.036	0.042	0.042	0.033
1080	0.070	0.146	0.066	0.063	0.102	0.061
1140	0.070	0.154	0.067	0.064	0.112	0.064
1200	0.071	0.160	0.069	0.067	0.120	0.067

List of Figures

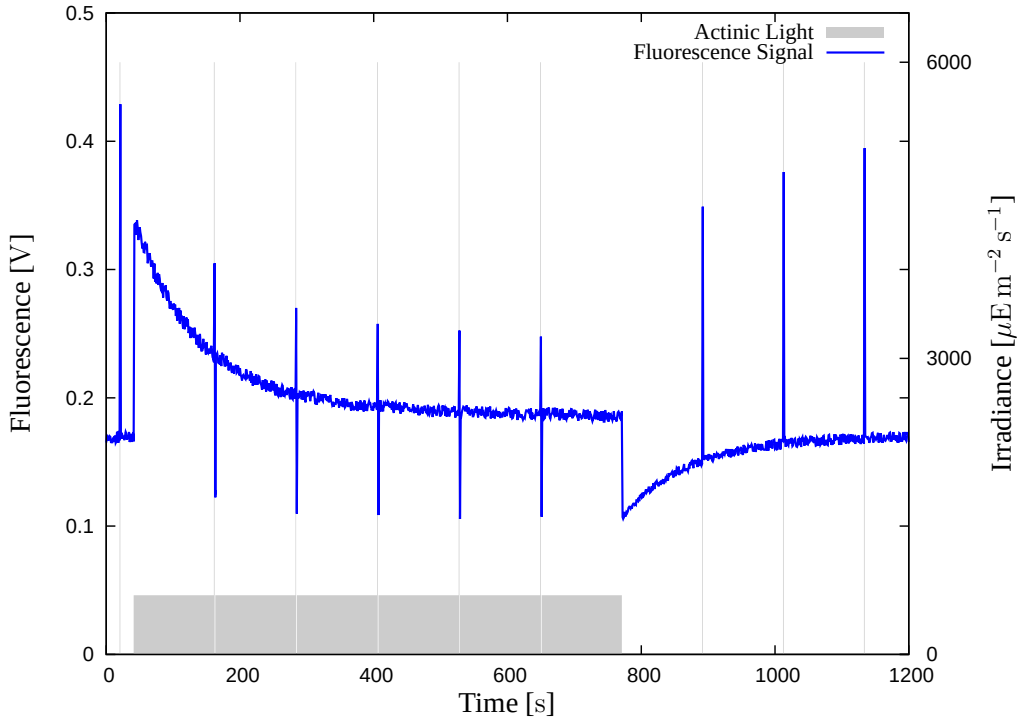

Figure 1: Representative PAM protocol and outcome. The light-gray lines represent the light irradiance, including both actinic and measuring lights; the darker line shows the corresponding fluorescence flux measurements (in volts).

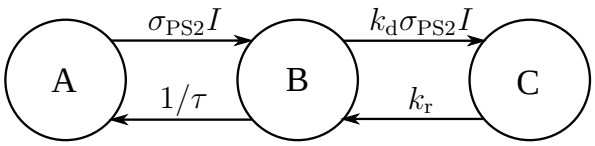

Figure 2: Schematic representation of the Han model

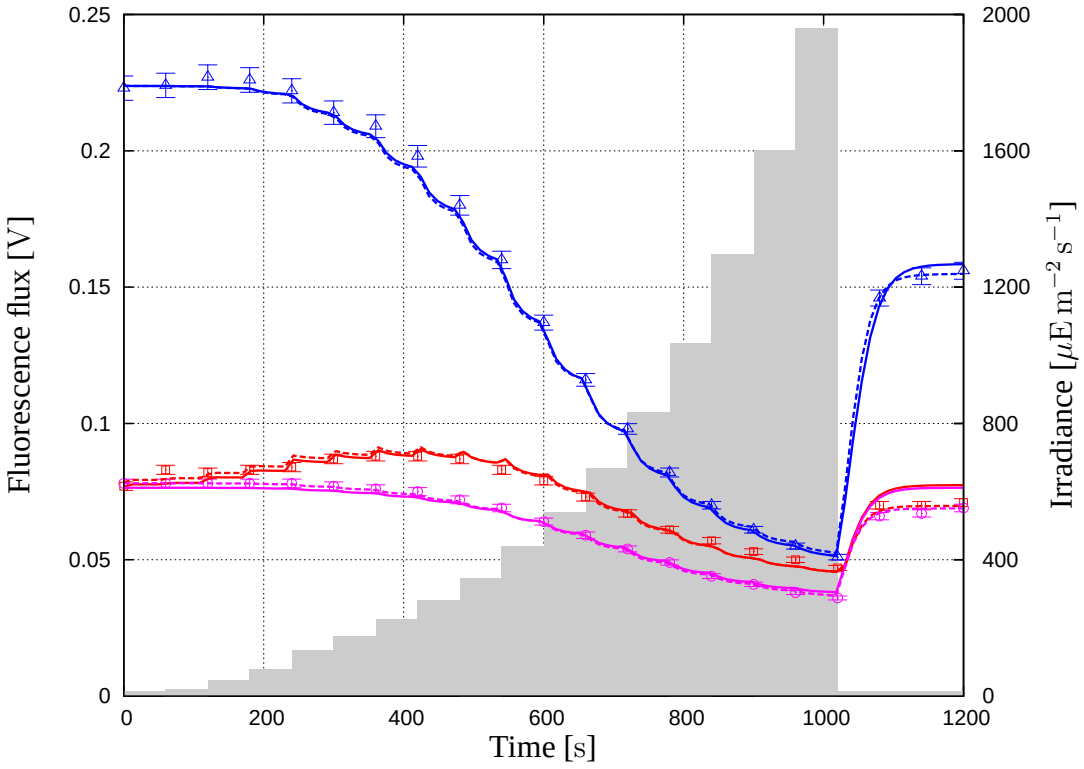

Figure 3: Comparison between the predicted and measured fluorescence fluxes F'_{m} (blue lines, triangles), F'_0 (purple lines, circles) and F' (red lines, square) in response to various actinic light levels I (gray-shaded area) for the calibration experiment. The dashed and continuous lines are obtained without and with the assumption $\Phi_{\mathrm{f}}^A = \Phi_{\mathrm{f}}^C$, respectively.

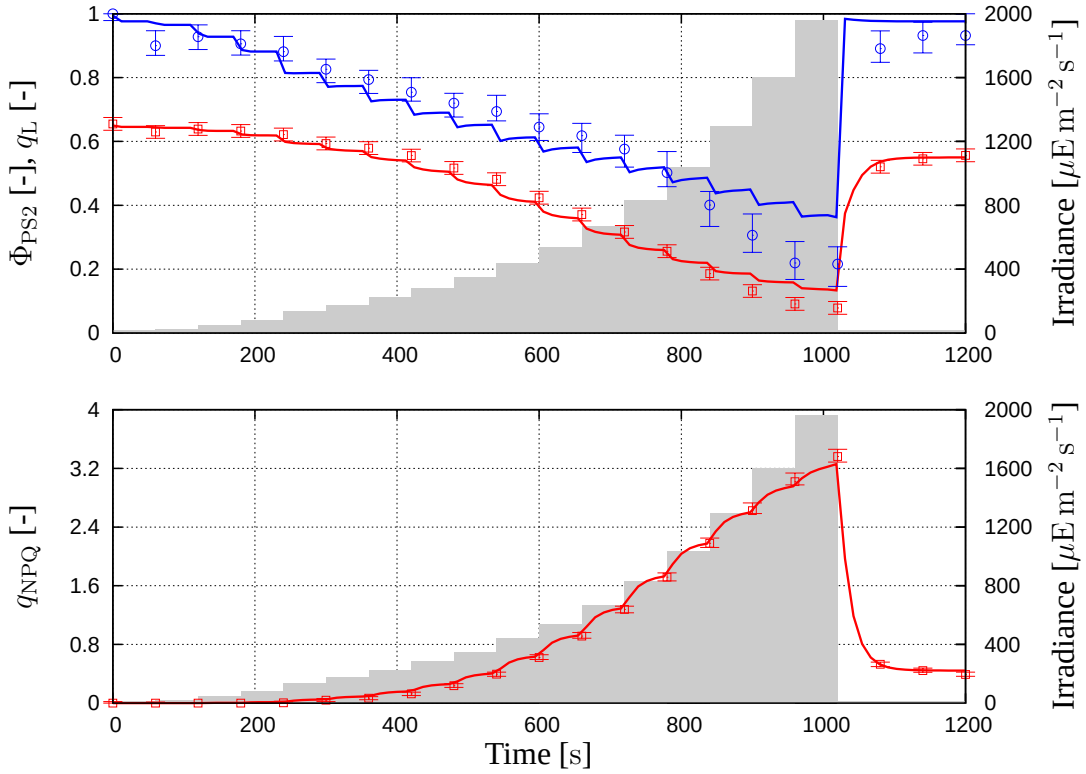

Figure 4: Upper plot: Comparison between the predicted and measured fluorescence indexes Φ_{PS2} (red lines, square) and q_L (blue lines, circles) at various actinic light levels I (grey-shaded area). Lower plot: Comparison between the predicted and measured fluorescence index q_{NPQ}.

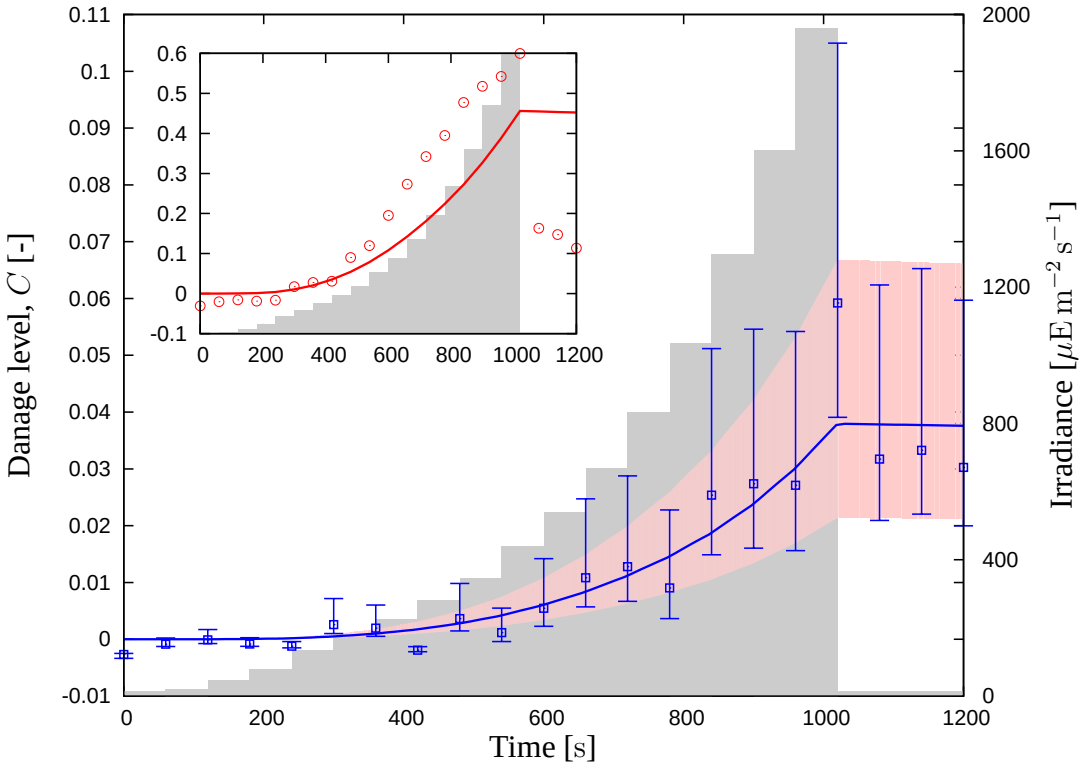

Figure 5: Large plot: Comparison between the fraction C of damaged RCIIs predicted by the full calibrated model (blue lines) and by the expression (19) (blue squares) at various actinic light levels I (grey-shaded area). Small plot: Similar comparison for an alternative model of qE-quenching (red lines and circles), whereby the qE-activity variable α affects the absorption cross section σ in (5) instead of the quantum yield of fluorescence Φ_{f}.

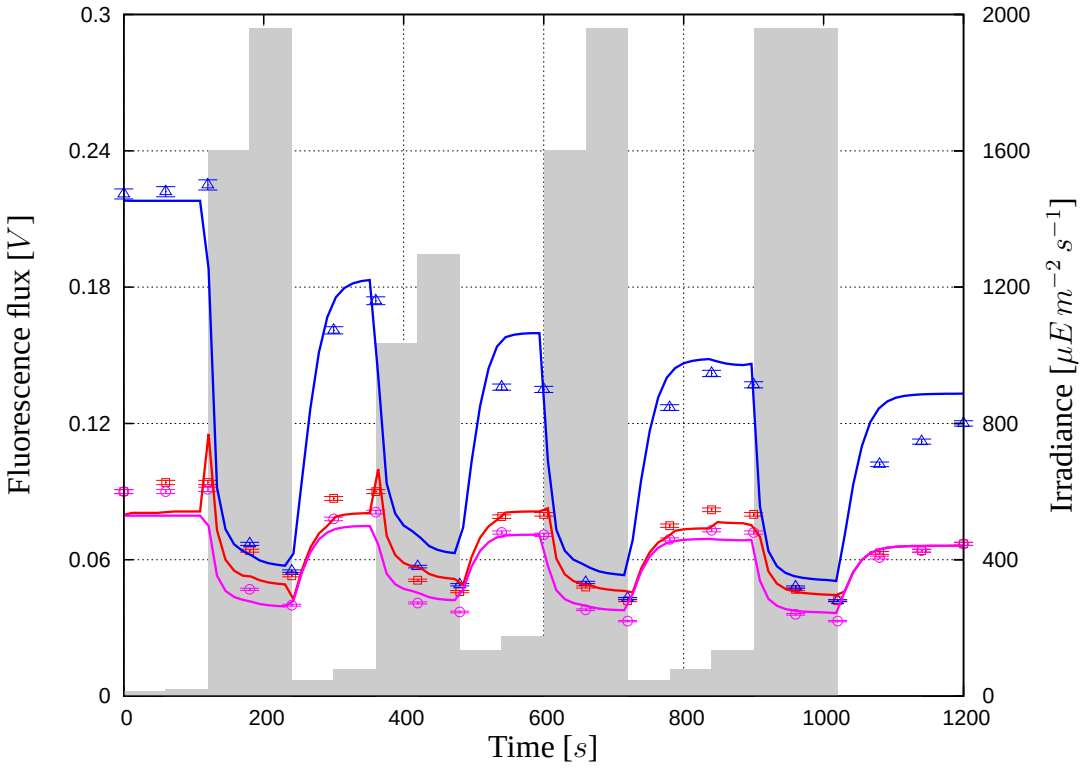

Figure 6: Comparison between the predicted and measured fluorescence fluxes F'_{m} (blue lines, triangles), F'_0 (purple lines, circles) and F' (red lines, square) in response to various actinic light levels I (gray-shaded area) for the validation experiment.